ARTICLES
PUBLISHED ONLINE: 28 AUGUST 2011 | DOI: 10.1038/NPHYS2073
nature physics

High-field superconductivity at an electronic topological transition in URhGe

E. A. Yelland[1,2]*, J. M. Barraclough[2], W. Wang[3], K. V. Kamenev[3] and A. D. Huxley[1,2]

The emergence of superconductivity at high magnetic fields in URhGe is regarded as a paradigm for new state formation approaching a quantum critical point. Until now, a divergence of the quasiparticle mass at the metamagnetic transition was considered essential for superconductivity to survive at magnetic fields above 30 T. Here we report the observation of quantum oscillations in URhGe revealing a tiny pocket of heavy quasiparticles that shrinks continuously with increasing magnetic field, and finally disappears at a topological Fermi surface transition close to or at the metamagnetic field. The quasiparticle mass decreases and remains finite, implying that the Fermi velocity vanishes due to the collapse of the Fermi wavevector. This offers a novel explanation for the re-emergence of superconductivity at extreme magnetic fields and makes URhGe the first proven example of a material where magnetic field-tuning of the Fermi surface, rather than quantum criticality alone, governs quantum phase formation.

The discovery and understanding of new quantum phases is a central theme of research in strongly correlated electron systems. Metals with narrow bandwidths, including the f-electron heavy fermion (HF) materials show rich behaviour because their high density of states (DOS) promotes correlation effects and the energy scale for navigating the phase diagram is accessible with realistic magnetic fields and pressures. The HF metals UGe_2 (ref. 1), URhGe (ref. 2) and UCoGe (ref. 3) attract particular interest because they show microscopic coexistence of superconductivity (SC) and ferromagnetism (FM), which are competing orders in conventional SC theories with opposite-spin pairs. They therefore offer the prospect of realizing the long-predicted metallic analogue of the A1 superfluid phase in ^{3}He (ref. 4), in which magnetic fluctuations bind together quasiparticles with equal spin. Strong experimental evidence that the Cooper pairs are indeed equal-spin states in URhGe is provided by the sensitivity of SC to disorder and the magnitude and T dependence of the critical field for destruction of SC (ref. 5).

The phase diagram of URhGe is shown schematically in Fig. 1. Ferromagnetism exists below $T = 9.5$ K with a spontaneous magnetic moment $M_c = 0.4\,\mu_B$ parallel to the crystal c-axis. Bulk SC forms deep within the FM state[2] at $T_c = 275$ mK in the cleanest crystals. A magnetic field applied along b first destroys SC, but remarkably it reappears between 8 T and ≈12.5 T with a higher T_c than at zero field[6]. Measurements with B tilted by an angle θ away from b within the easy bc-plane[6] suggest the surface of first order transitions separating $M_c > 0$ from $M_c < 0$ bifurcates at a tricritical point around 12 T, giving two surfaces $B_R(\pm\theta, T)$ across which the moment rotates discontinuously towards B. These surfaces extend to angles a few degrees away from b, beyond which the transition is replaced by a crossover. Although re-entrant superconductivity in other materials can be explained by Jaccarino–Peter compensation between internal and external fields, this explanation has been ruled out for URhGe (ref. 6). Instead, the presence of quantum critical points at the end of the first order lines suggests that critical magnetic fluctuations provide the pairing interaction.

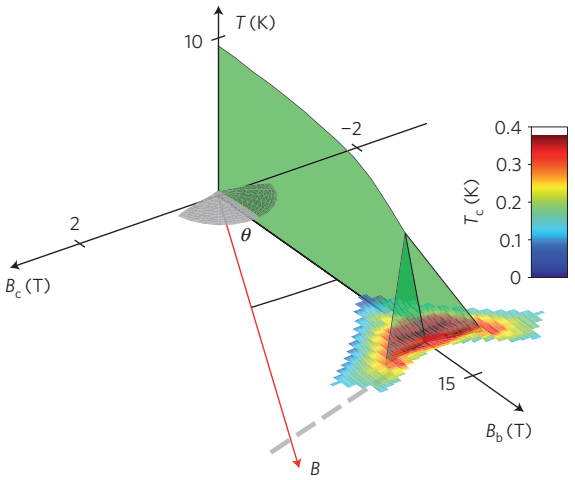

Figure 1 | Schematic phase diagram of URhGe for magnetic fields applied in the crystallographic *bc*-plane. Below 9.5 K URhGe is ferromagnetic with its moment parallel to the *c*-axis. An applied magnetic field causes the moment to rotate towards the field direction; changes are smooth except when crossing one of the sheets where a first order moment-rotation transition occurs. Two regions of superconductivity exist: one at low field and another at high field surrounding the point where the three transition surfaces meet. Our quantum oscillation results reveal a Fermi surface transition across the dashed line at $\theta = 10°$.

Here we report the direct observation of the Fermi surface (FS) in URhGe through the Shubnikov–de Haas (SdH) effect, providing precise information on the FS geometry and quasiparticle mass in a crucial part of the phase diagram. The magnetic field dependence of the quantum oscillation (QO) frequency and amplitude, and the quasiparticle mass, together with a non-Fermi liquid form for the resistivity, suggest that one or more Fermi surface pockets vanish at a zero-temperature field-induced topological

[1]Scottish Universities Physics Alliance (SUPA), School of Physics and Astronomy and Centre for Science at Extreme Conditions, University of Edinburgh, Mayfield Road, Edinburgh EH9 3JZ, UK, [2]SUPA, School of Physics and Astronomy, University of St Andrews, North Haugh, St Andrews KY16 9SS, UK, [3]School of Engineering and Centre for Science at Extreme Conditions, University of Edinburgh, Mayfield Road, Edinburgh EH9 3JZ, UK.
*e-mail: eay1@st-andrews.ac.uk.

transition, also known as a Lifshitz transition (LT). A simple model consistent with our observations gives an orbital-limiting field that can explain the field extent of the re-entrant SC in quantitative agreement with experiment.

Our magnetoresistance measurements were made on a single crystal of URhGe with a residual resistance ratio $\rho(300\,\mathrm{K})/\rho(T\to 0\,\mathrm{K}) = 130$, indicating a high degree of crystalline order (see Methods). Figure 2 shows the angle dependence of $R(B)$ as B is rotated from b ($\theta = 0°$) towards c with $T \approx 100$ mK. For $B \parallel b$, a SC pocket exists in the range $8.5 \le B \le 12.5$ T (ref. 6). On rotating B towards c, the B-width of the zero-resistance region shrinks continuously, reaching zero at $\theta \approx 5.5°$. By $\theta = 6°$, a Fast Fourier transform (FFT) in $1/B$ of $R(B)$ reveals a sharp peak at $F = 555$ T that reaches a maximum amplitude at $\theta = 10°$. The periodicity and T dependence of the oscillations are characteristic of QOs that occur at high magnetic fields in clean samples when the electronic states become confined to Landau tubes[7].

Quantum oscillations in resistivity, also called SdH oscillations, stem principally from the modulation of the electronic scattering rate[7]. A quantum mechanical treatment of electron scattering at high magnetic field for a three-dimensional metal[8] leads to

$$\tilde{\rho}/\rho \approx \alpha R_T |\tilde{n}(\epsilon_F)|/n(\epsilon_F)$$

$$R_T = \frac{2\pi^2 k_B m^* T/e\hbar B}{\sinh(2\pi^2 k_B m^* T/e\hbar B)} \qquad (1)$$

where $\tilde{\rho}$ and $\tilde{n}(\epsilon_F)$ are the oscillatory amplitudes of the resistivity ρ and DOS $n(\epsilon_F)$ arising from the passage of Landau tubes through a particular extremal cross-section of the Fermi surface; α is a number ~ 1 depending on the scattering mechanism and R_T describes the attenuation of the oscillations due to thermal broadening of the Landau levels. R_T is important because it allows the enhanced quasiparticle mass m^* to be determined, providing an experimental probe of the same many-body interactions that enhance the specific heat. The fundamental component of $\tilde{n}(\epsilon_F)$ is given by the Lifshitz–Kosevich (LK) formula[7]

$$\tilde{n}(\epsilon_F) \propto \frac{B^{\frac{1}{2}} R_D}{\sqrt{\partial^2 \mathcal{A}/\partial k_\parallel^2}} \cos\left[\frac{2\pi F(B)}{B} + \phi\right] \qquad (2)$$

where $\mathcal{A}$ is the area of the orbit in k-space, B is the magnetic induction, R_D is the Dingle factor describing damping due to scattering and $F(B) = (\hbar/2\pi e)\mathcal{A}(B)$ is the QO frequency. The curvature factor $\partial^2\mathcal{A}/\partial k_\parallel^2$ accounts for the number of k-states that coherently contribute to the oscillatory amplitude. For ferromagnets such as URhGe the spontaneous splitting of the FS in zero applied magnetic field means that each quantum oscillation frequency derives from a single spin species; whether each spin species produces an observable quantum oscillation component depends on the topology, scattering rate and quasiparticle masses on the separate sheets, which could differ markedly in a strongly polarized ferromagnet.

The FFTs of our resistivity measurements for URhGe in Fig. 2b show a clear peak at $F = 555$ T, well separated from spectral weight below 200 T (see Supplementary Information). This quantum oscillation component is the focus of our analysis. The frequency corresponds to a Fermi surface cross-section with a zero-field-projected area $\mathcal{A} = 0.053$ Å^{-2}, 7% of the Brillouin zone (BZ) area. The absence of any resolvable angle dependence of F in Fig. 2b provides an upper limit $|F(20°) - F(0°)| \le 10$ T that excludes a locally 2D FS region or a FS neck. The data are consistent with a spherical or ellipsoidal pocket that is almost circular in the bc-plane, and in the first case the pocket's small size means that it would contain only $\pi k_F^3/(3a^*b^*c^*) = 2.1\times10^{-3}$ carriers per U, where k_F is the Fermi wavevector of the pocket.

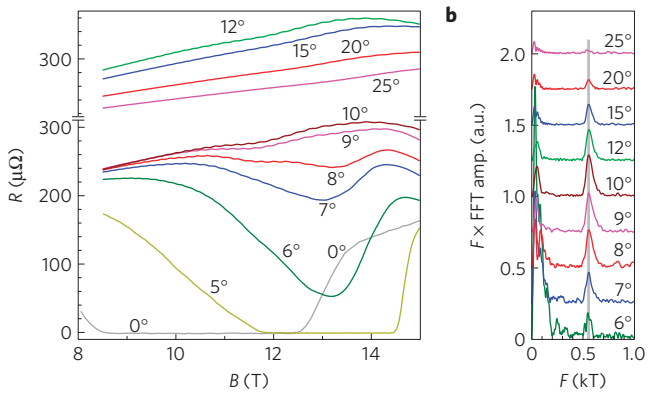

Figure 2 | Field-angle dependence of $R(B)$ at $T \approx 100$ mK. a, Raw data for various angles θ. The ripples visible at $\theta = 10°$ are Shubnikov-de Haas oscillations. **b**, Fast Fourier transform of $R(B)$ in the range $8.5 \le B \le 15.0$ T after subtracting a linear background (offset vertically for clarity). The oscillations give a sharp peak marked by the vertical line at $F = 555$ T. This reaches a maximum amplitude at 10°, where R is also maximum, before disappearing at higher angles.

The temperature dependence of $R(B)$ is shown in Fig. 3a,b at $\theta = 8°$ and $\theta = 10°$, where the QO signal is strongest. We have extracted the amplitude envelope of the oscillating part of $R(B)$ as a function of B and T (see Supplementary Information). The T-dependent amplitude at fixed B was then fitted to R_T in equation (1), as shown for representative values of B in Fig. 3c. The fits provide the quasiparticle mass $m^*(B)$ shown in Fig. 3d, which decreases from $\approx 22m_e$ at 8 T to $\approx 12m_e$ at 15 T. For a spherical pocket, the contribution to the low-temperature linear coefficient in the specific heat, γ, is $\gamma = n_s(k_B^2/6\hbar^2)k_F m^*$ per unit volume, where n_s is the number of copies of the FS sheet in the BZ and there is no spin degeneracy. For $m^* = 20m_e$ and $\mathcal{A} = 0.053$ Å^{-2}, $\gamma_{QO} = 2.3$ mJ mol^{-1} K^{-2} per sheet. There are no measurements of the heat capacity at this field angle for comparison, but magnetization[9] and a.c. calorimetry measurements[10] suggest that the total heat capacity coefficient at 9 T and $\theta \approx 0°$ is little different from the zero-field value $\gamma_{TOT} = 160$ mJ mol^{-1} K^{-2} (ref. 2). As the contribution from the pocket(s) we observe is a lot smaller than this, other Fermi surfaces not detected in our study must be present. The large longitudinal magnetic susceptibility suggests that at least one of these undetected sheets must be of the opposite spin.

In the standard Fermi liquid description of the metallic state, the linear term in the specific heat is closely connected to the A coefficient in the low-temperature electrical resistivity $\rho = \rho_0 + AT^2$. Generally, $\gamma \propto m^*$, whereas $A \propto m^{*2}$. In our measurements on URhGe at $\theta = 10°$, we find that the T dependence of the non-oscillatory background resistivity does indeed weaken with field as m^* decreases, but it does not have the usual Fermi liquid form and therefore cannot be simply related to changes of the electronic heat capacity. It was reported[11] in UCoGe that m^* also decreases with increasing field simultaneously as the T dependence of the resistivity weakens, but in that case the resistivity did follow a Fermi liquid form. For $B \to 0$ T in URhGe the usual Fermi liquid form is recovered above T_c, but strong deviations occur at high field where distinct low-temperature ($T < T^*$) and high-temperature ($T > T^*$) regions exist that have nearly linear and super-linear T dependences, as in Fig. 3b (inset) at 13 T. The crossover temperature $T^* \lesssim 0.4$ K for all fields. If a T^2 temperature dependence is imposed to fit the data, as illustrated by the dash–dotted curve in the inset of Fig. 3b, the experimental resistivity has an initial upward deviation from this form with decreasing temperature as well as a subsequent sharp downturn below T^*. The upturn is present at all fields and therefore cannot be attributed

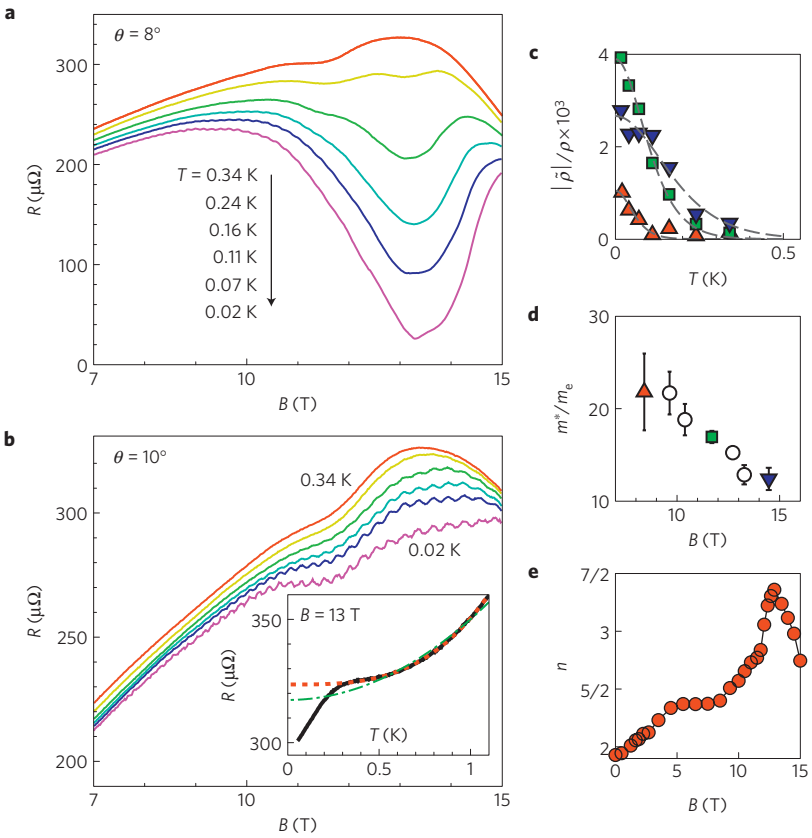

Figure 3 | Temperature dependence of the quantum oscillations. a,**b**, $R(B)$ at $\theta = 8°$ and 10° for various T. Inset: $R(T)$ at 10° and 13 T (solid curve) with fits described in the text. **c**, QO amplitude versus T for the 10° data at selected values of B (symbols) and fits to the Lifshitz–Kosevich form (dashed lines). **d**, The B dependence of the quasiparticle mass m^*. The values are obtained from the fits in **c** and the error bars indicate the uncertainty estimated from these fits. **e**, Exponent n from fits of $R(T)$ to $\rho = \rho_0 + AT^n$ for $0.4 \leq T \leq 1.1$ K at $\theta = 10°$.

to low-frequency QOs, which would give contributions to the resistivity that oscillate from positive to negative as a function of field; a simple T^2 dependence above T^* in combination with QOs cannot therefore explain our data. In contrast, a fit of the form $\rho - \rho_0 \propto T^n$, with n free to vary, describes the data well in the higher T region ($0.4 \leq T \leq 1.1$ K). In this case only the downturn below T^* requires additional explanation. The continuous evolution with angle of the slow undulations in Fig. 2 to a state that is almost resistanceless at 20 mK and $\theta = 8°$ (Fig. 3a), and is resistanceless for smaller θ, hints that the behaviour below T^* relates strongly to the proximity to SC, for example, a partial transition into a superconducting state. Applying the floating-power fit yields the exponents shown in Fig. 3e: $n = 2.0$ at zero field, but n increases to ≈2.4 at 8 T before jumping sharply to ≈3.4 at 13 T and then decreasing again beyond the magnetic crossover field. A non-T^2 power law with $n = 5/2$ or $7/2$ is consistent with proximity to a field-induced 3D LT (refs 12–14).

The magnetic field dependence of R at $T = 20$ mK is shown in Fig. 4 up to 17 T. The QO component centred on 555 T has been isolated from the B-dependent background by subtraction of a smooth function (residuals shown in Fig. 4b). There are > 30 consecutive oscillations resolvable in the range $8.2 \leq B \leq 15.5$ T, allowing a precise comparison with the LK theory equations (1) and (2). An LK model calculation (details in Supplementary Information) is shown in Fig. 4b. The oscillating part of the model expression contains three adjustable parameters controlling the oscillation phase, frequency and the B dependence of the frequency. Crucially, the accurate phase relation between fit and data over the entire range of B can only be achieved by including a B-dependent term in the frequency. In a paramagnet $F(B)$ in equation (2) depends linearly on B and can be replaced by $F(0)$ with the B-linear part absorbed in the QO phase. However, B-dependent QO frequencies are expected in any itinerant magnet in which M varies nonlinearly with B and have been observed in a number of f- and d-electron materials, both FM and non-FM, for example UPt_3 (ref. 15), $ZrZn_2$ (ref. 16), $Sr_3Ru_2O_7$ (ref. 17), and $YbRh_2Si_2$ (ref. 18). Our observed QO frequency F_{obs} is shown in Fig. 4c. In this plot we have accounted for the small difference between the applied magnetic field and the internal field that enters equation (2) using $M(B)$ of URhGe measured at angles close to those reported here[6]; this correction changes the frequency by <15 T and is therefore negligible on the scale of the observed field dependence. The actual FS cross-sectional area $\mathcal{A}(B)$ is related to F_{obs} by $F_{obs}(B) \propto \mathcal{A}(B) - B\mathrm{d}\mathcal{A}/\mathrm{d}B$ (ref. 15). Figure 4d shows forms of $\mathcal{A}(B)$ that are consistent with F_{obs}, differing from each other only in the value of the undetermined B-linear term. The lowest curve for $\mathcal{A}(B)$ shows it reaching zero at 15.5 T, where we suggest a magnetic field-induced LT occurs; this provides a natural explanation for the sudden loss of oscillatory signal at high field.

The dependence of the QO amplitude on B contains information about quasiparticle scattering through a mean free path ℓ_Q that enters the Dingle factor $R_D = \exp(-\pi\sqrt{2\hbar F/e}/B\ell_Q)$ in equation (2). Comparing the amplitude envelope of the oscillatory data in Fig. 4b to the LK model with $\ell_Q = 550$ Å and $\mathcal{A} = 0.043$ Å^{-2}, independent of B, we see that the model tracks the data up to ~11 T, but at higher B the oscillations rapidly become weaker than predicted and are absent within experimental resolution at and above 15.5 T. Note that the effect of the decrease in the background resistance above 15 T is included in the calculation. The lower curve shows the LK result for the case of a LT, where $\mathcal{A}(B)$ is

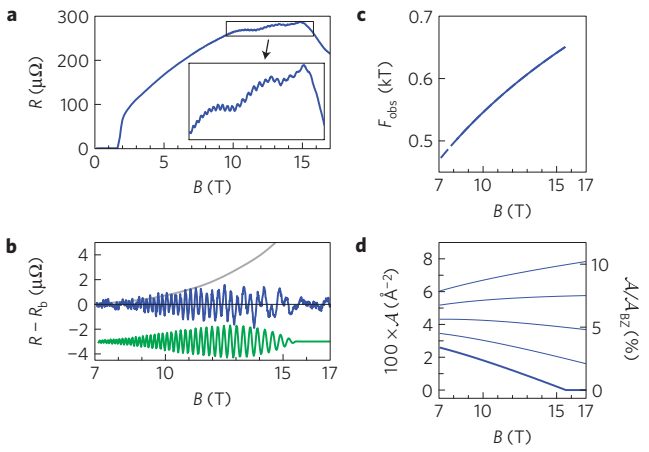

Figure 4 | Magnetic field dependence of the quantum oscillations. a, $R(B)$ at $T = 20$ mK for $B \leq 17$ T and $\theta \approx 10°$. The oscillations disappear suddenly at $B \approx 15.5$ T where the non-oscillatory part of R also drops sharply. **b**, Residual after subtracting a smoothly varying background (blue curve) and Lifshitz–Kosevich model calculations for a Fermi surface orbit that shrinks to zero size (green curve) and the amplitude envelope expected for a constant orbit size (grey curve). **c**, Observed quantum oscillation frequency $F_{obs}(B)$. **d**, Forms of the B-dependent Fermi surface area that are consistent with $F_{obs}(B)$. The bold line shows $\mathcal{A}(B)$ vanishing at 15.5 T corresponding to a LT where a Fermi pocket shrinks to a point or a neck pinches off.

given by the lowest curve in Fig. 4d. Using a B-independent mean free path $\ell_Q = 550 \pm 100$ Å, the calculated QO amplitude is in good agreement with experiment over the entire range of B (see Supplementary Information for further details of the calculation). Physically the loss of amplitude occurs both because carriers are slowing down approaching the LT and because they are diminishing in number. Without attempting to capture the details of multi-band magnetotransport, this simple argument shows that a B-induced decrease of the Fermi wavevector culminating in the disappearance of the pocket at a LT can explain the otherwise anomalous B-dependent QO amplitude. Other potential explanations can be eliminated, as described in the Supplementary Information.

To examine whether our data are consistent with a Zeeman-driven LT we consider for definiteness a vanishing pocket of minority spin electrons, but the discussion also applies to majority spin holes. As B is increased, the Fermi level relative to the bottom of the pocket decreases, and its B-derivative $\partial(\epsilon_F - \epsilon_0)/\partial B = 2\mu_{eff}$ can be used to estimate μ_{eff}, the component of the effective electronic moment parallel to the field. The factor of 2 applies when the Fermi level is effectively pinned by a dominant DOS on the majority spin band. We consider two possibilities: (1) the density of states of the pocket-band is unaffected as $\epsilon_F - \epsilon_0$ changes with field, giving $2\mu_{eff} = (1/m^*)\partial\mathcal{A}/\partial B$; (2) the bandwidth renormalization changes with field but the band maintains a parabolic dispersion for which $2\mu_{eff} = \partial(\mathcal{A}/m^*)/\partial B$. The true case might lie between these two extremes. The QO results provide both $\mathcal{A}(B)$ and an enhanced quasiparticle mass $m^*(B) = (\hbar^2/2\pi)\mathrm{d}\mathcal{A}/\mathrm{d}E$. For both cases we find μ_{eff} is small at low field, where the component of the magnetic moment $\|B$ is known to be small, but it increases to $\approx 3\,\mu_B$ at 15 T, where the moment has rotated towards the field direction. This value is approximately a factor of two larger than expected for U moments[19], but would be in good agreement for a Wilson ratio of two, appropriate for the Kondo effect in which the susceptibility enhancement is a factor two larger than the DOS enhancement. The relationship between the field- and energy-scale of the unusual features in our QO data thus strongly supports the interpretation in terms of a LT.

We now discuss the consequences of our findings for field-induced superconductivity. In an equal-spin-paired superconductor the upper critical field is expected to be orbitally limited to a value $B_{c2}^{orb} = \Phi_0/(2\pi\xi^2)$, where ξ is the superconducting coherence length. This is the maximum field that a type II superconductor can sustain in its mixed state before the normal cores of the flux vortices occupy the entire volume and superconductivity is destroyed. It was shown in ref. 20 that the observed critical fields of both low- and high-field superconductivity can be explained by a smooth, continuous magnetic field dependence of $1/\xi^2$ that is strongly peaked approaching the metamagnetic transition. In Bardeen–Cooper–Schrieffer (BCS) theory $\xi = \hbar v_F/\pi\Delta$, where Δ measures the excitation gap in the SC state and $v_F = \hbar k_F/m^*$ is the Fermi velocity. This shows that the required reduction in ξ can occur if v_F vanishes approaching the transition, for example due to a divergence of m^*, as has been widely considered. Our present finding that k_F vanishes provides an alternative explanation for the field dependence of ξ, which we now examine quantitatively. Figure 5a shows v_F for the shrinking Fermi pocket calculated from the experimental values of k_F and m^*. The values are low and decrease from 4.4×10^3 m s^{-1} at 9 T to zero at the LT. In a superconductor with multiple Fermi surface sheets, it is likely at sufficiently high magnetic fields that the superconducting coherence length ξ would be associated with the sheet with the lowest Fermi velocity, provided that Δ is not compensatingly larger on other sheets. To estimate ξ for the Fermi pocket in absolute units we take $\Delta = 2\,k_B T_c$, with $T_c(B)$ chosen to interpolate linearly between the measured zero-field value and the observed maximum value of 0.45 K at 12 T for $B \| b$. The resulting orbital-limiting field diverges on approaching the LT, as shown in Fig. 5b. For $\theta = 10°$, where we know v_F from the QOs, the orbital-limiting field just fails to exceed the applied field up to a cut-off at $k_F\xi = 1$, beyond which the BCS expression for ξ cannot be applied. This is consistent with the observed absence of SC at high B at 10°. To predict what could occur at $\theta = 0°$, we force $\mathcal{A}(B)$ to vanish at 13 T, where the high-B SC is destroyed. The resulting $\xi(B)$ leads to a region at high field in Fig. 5c where B_{c2}^{orb} exceeds B and equal-spin-paired SC is not prevented by orbital limiting. This calculation uses a B-independent mass $m^* = 40m_e$ (further details are in the Supplementary Information). The absolute magnitude and B dependence are remarkably close to experimental values of the superconducting B_{c2} (ref. 20), suggesting that the slowing down of quasiparticles at a LT would allow superconductivity to survive above 30 T, without a divergence of the quasiparticle mass.

Our results show that the destruction of the low-field superconductivity, and its sudden re-emergence at high field, is consistent with a weak, continuous field dependence of the pairing strength. This strongly suggests that the same pairing mechanism drives superconductivity in the two regions and that the enhancement of pairing due to critical fluctuations near the magnetic transition need not be strongly peaked as a function of magnetic field applied parallel to the b-axis. The dominant role of a very small Fermi surface pocket in producing high-field superconductivity is unexpected and motivates further investigation of multi-band effects in URhGe. Multi-band superconductivity has been widely studied in MgB_2, a BCS superconductor with a conventional scalar order parameter in which opposite spins are paired; the behaviour in URhGe could be much richer, because in addition to the strong field evolution of the Fermi-surface, its order parameter has a spin structure permitting pairing on strongly spin-split Fermi surfaces, but with a lower spatial symmetry than the crystal structure, making it fragile to disruption by non-magnetic scattering of electrons.

Recent experiments on $CeRu_2Si_2$ (ref. 21) suggest that the field-induced metamagnetic transition in this material is also associated with a sheet of the Fermi surface shrinking continuously to zero size and the same physics may underlie the field-induced

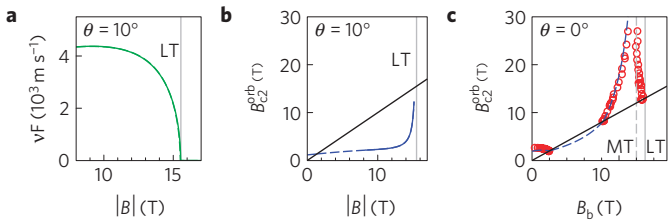

Figure 5 | Magnetic field dependence of the Fermi velocity v_F and orbital-limiting field B_{c2}^{orb} for the Fermi pocket detected in this study. **a**, $v_F(B) = \hbar k_F/m^*$ with k_F and m^* determined by quantum oscillations at $\theta = 10°$. $v_F \to 0$ at the LT, where $k_F \to 0$. **b**, $B_{c2}^{orb} = \Phi_0/2\pi\xi^2$ at $\theta = 10°$ calculated from v_F (solid curve; dashed curve uses extrapolated values of k_F and m^*). High-B superconductivity cannot occur because $B_{c2}^{orb} < |B|$. **c**, Calculated B_{c2}^{orb} at $\theta = 0°$ if a LT occurs at 13 T for a B-independent mass $m^* = 40\,m_e$ (dashed line). MT marks the magnetic transition. Now $B_{c2}^{orb} > B_b$ at high B so orbital limiting does not destroy superconductivity for $8 \lesssim B_b \lesssim 13$ T. Symbols show measured values of the superconducting B_{c2} (ref. 20), which are remarkably well described by the model.

transition to antiferromagnetism in $YbRh_2Si_2$ (refs 14,22). In both these cases the LT separates two phases (both Fermi liquids in the low-T limit) but new state formation around the transition has not been observed. Our results on URhGe provide the first example where the presence of a LT enables phase formation in the vicinity of a quantum critical point (QCP), in this case by creating conditions favourable for high-field superconductivity. It remains an open question whether the Liftshitz transition also plays a role in shaping the spectrum of magnetic fluctuations responsible for superconducting pairing in URhGe. This highlights the need for a theory of superconductivity in URhGe that includes the effects of a LT alongside quantum criticality, addressing both the changes to the spectrum of magnetic fluctuations[23] and the existence of critically slow fermionic quasiparticles. More generally, topological transitions of the Fermi surface may be commoner than presently thought in narrow-band metals and may offer a route to quantum phase formation that deserves more attention.

Methods

The single crystal sample was cut from an ingot made by rapidly cooling a stoichiometric molten mixture of the elements under purified argon in a water-cooled copper crucible followed by annealing under ultra-high vacuum for one week at 900 °C. The single crystal was carefully examined and oriented by X-ray Laue diffraction. Magnetoresistance measurements were made using two different set-ups. The first used piezoelectric rotators to control the field angle with relative precision ∼0.02° about two axes for $T \gtrsim 80$ mK and $B \leq 17$ T with a field-calibrated RuO_2 resistance thermometer mounted next to the sample. In the second set-up the sample was aligned by Laue diffraction and rigidly mounted to a stage that was strongly thermally coupled to a zero-field thermometer. This provided a cross-check on the in-field thermometry of the first set-up and allowed temperatures down to 20 mK. A standard a.c. lock-in technique and a low-temperature transformer were used, giving sensitivity to QO signals of amplitude $\geq 60\,n\Omega \cong 3$ pV; the measurement current was always $\leq 100\,\mu A$.

Received 8 April 2011; accepted 27 July 2011; published online 28 August 2011

References

1. Saxena, S. S. *et al.* Superconductivity on the border of itinerant electron ferromagnetism in UGe_2. *Nature* **406,** 587–592 (2000).
2. Aoki, D. *et al.* Coexistence of superconductivity and ferromagnetism in URhGe. *Nature* **413,** 613–616 (2001).
3. Huy, N. T. *et al.* Superconductivity on the border of weak itinerant ferromagnetism in UCoGe. *Phys. Rev. Lett.* **99,** 067006 (2007).
4. Fay, D. & Appel, J. Coexistence of *p*-state superconductivity and itinerant ferromagnetism. *Phys. Rev. B* **22,** 3173–3182 (1980).
5. Hardy, F. & Huxley, A. D. *p*-wave superconductivity in the ferromagnetic superconductor URhGe. *Phys. Rev. Lett.* **94,** 247006 (2005).
6. Lévy, F., Sheikin, I., Grenier, B. & Huxley, A. D. Magnetic field-induced superconductivity in the ferromagnet URhGe. *Science* **309,** 1343–1346 (2005).
7. Shoenberg, D. Magnetic Oscillations in Metals (Cambridge Univ. Press).
8. Adams, E. N. & Holstein, T. D. Quantum theory of transverse galvanomagnetic phenomena. *J. Phys. Chem. Solids* **10,** 254–276 (1959).
9. Aoki, D. *et al.* Superconductivity reinforced by magnetic field and the magnetic instability in uranium ferromagnets. *J. Phys. Soc. Jpn* **80,** SA008 (2011).
10. Lévy, F., Sheikin, I., Grenier, B., Marcenat, C. & Huxley, A. Coexistence and interplay of superconductivity and ferromagnetism in URhGe. *J. Phys. Condens. Matter* **21,** 164211 (2009).
11. Aoki, D. *et al.* First observation of quantum oscillations in the ferromagnetic superconductor UCoGe. *J. Phys. Soc. Jpn* **80,** 013705 (2011).
12. Blanter, Y. M., Kaganov, M. I., Pantsulaya, A. V. & Varlamov, A. A. The theory of electronic topological transitions. *Phys. Rep.* **245,** 159–257 (1994).
13. Katsnelson, M. I. & Trefilov, A. V. Fermi-liquid theory of electronic topological transitions and screening anomalies in metals. *Phys. Rev. B* **61,** 1643–1645 (2000).
14. Hackl, A. & Vojta, M. Zeeman-driven Lifshitz transition: A model for the experimentally observed Fermi-surface reconstruction in $YbRh_2Si_2$. *Phys. Rev. Lett.* **106,** 137002 (2011).
15. Julian, S. R., Teunissen, P. A. A. & Wiegers, S. A. J. Fermi surface of UPt_3 from 3 to 30 T: Field-induced quasiparticle band polarization and the metamagnetic transition. *Phys. Rev. B* **46,** 9821–9824 (1992).
16. van Ruitenbeek, J. M. *et al.* A de Haas–van Alphen study of the field dependence of the Fermi surface in $ZrZn_2$. *J. Phys. F* **12,** 2919–2928 (1982).
17. Mercure, J-F. *et al.* Quantum oscillations near the metamagnetic transition in $Sr_3Ru_2O_7$. *Phys. Rev. B* **81,** 235103 (2010).
18. Rourke, P. M. C. *et al.* Magnetic-field dependence of the $YbRh_2Si_2$ Fermi surface. *Phys. Rev. Lett.* **101,** 237205 (2008).
19. Freeman, A. J., Desclaux, J. P., Lander, G. H. & Faber, J. Neutron magnetic form factors of uranium ions. *Phys. Rev. B* **13,** 1168–1176 (1976).
20. Lévy, F., Sheikin, I. & Huxley, A. Acute enhancement of the upper critical field for superconductivity approaching a quantum critical point in URhGe. *Nature Phys.* **3,** 460–463 (2007).
21. Daou, R., Bergemann, C. & Julian, S. R. Continuous evolution of the Fermi surface of $CeRu_2Si_2$ across the metamagnetic transition. *Phys. Rev. Lett.* **96,** 026401 (2006).
22. Kusminskiy, S. V., Beach, K. S. D., Neto, A. H. C. & Campbell, D. K. Mean-field study of the heavy fermion metamagnetic transition. *Phys. Rev. B* **77,** 094419 (2008).
23. Yamaji, Y., Misawa, T. & Imada, M. Quantum metamagnetic transitions induced by changes in Fermi-surface topology: Applications to a weak itinerant-electron ferromagnet $ZrZn_2$. *J. Phys. Soc. Jpn* **76,** 063702 (2007).

Acknowledgements

The sample studied was derived from material kindly supplied by the CEA-Grenoble. Research support was provided by the Engineering and Physical Sciences Research Council and the Royal Society.

Author contributions

E.A.Y. set up and made the measurements, analysed the data and wrote the manuscript with input from A.D.H. J.M.B. contributed to the data acquisition and analysis. W.W. and K.V.K. designed the 2-axis rotator stage.

Additional information

The authors declare no competing financial interests. Supplementary information accompanies this paper on www.nature.com/naturephysics. Reprints and permissions information is available online at http://www.nature.com/reprints. Correspondence and requests for materials should be addressed to E.A.Y. or A.D.H.